JOURNAL OF APPLIED ELECTROCHEMISTRY **26** (1996) 161–170

Bulk copper electrodeposition on gold imaged by *in situ* STM: morphology and influence of tip potential

J. E. T. ANDERSEN*, G. BECH-NIELSEN and P. MØLLER

Centre of Advanced Electroplating, The Technical University of Denmark, Building no. 425, DK-2800 Lyngby, Denmark

J. C. REEVE

Chemical Laboratory A, The Technical University of Denmark, Building no. 207, DK-2800 Lyngby, Denmark

Received 29 November 1993; revised 5 June 1994

Electrochemical measurements were carried out simultaneously with acquisition of *in situ* STM images of copper electrodeposition at low cathodic overpotentials and subsequent dissolution from the underlying polycrystalline gold surfaces. The morphologies of the copper deposits were examined for correlation with features of the current–voltage diagram. Copper growth is by nucleation and formation of 3D islands. During the initial stages of bulk copper growth the potentials were fixed at selected values and a balance observed between formation of polycrystalline copper nuclei and of copper crystals. After the first cycle of copper deposition and dissolution the morphology of the polycrystalline gold surface had apparently changed into a recrystallized phase of a copper-gold alloy. At a given stage of the cycle the potential of the electrode was found to depend linearly on the tip potential. In a wide range of tip potentials the onset of copper deposition and end of dissolution showed a potential separation of 59 ± 5 mV indicating a single electron process.

1. Introduction

One of the most important recent tools developed for the study of electrochemical processes is the technique of *in situ* STM (scanning tunnelling microscopy) which is one of a series of new techniques generally known collectively as scanning probe microscopy (SPM). The techniques have revolutionized the study of electrodes [1]. Compared with STM for air and nonelectrolyte studies, the *in situ* STM technique is more difficult to operate, because it requires independent and simultaneous control of the tip potential and the potential of the working electrode with respect to a common reference electrode [2]. The advantage of *in situ* STM is that it can provide atomic resolution of surfaces where electrode processes are in progress. For example it allows atomic level real time studies of underpotential deposition (UPD) [3]. In experiments with *in situ* STM one always has to consider the influence of the tip which to some extent impedes the diffusion of ions through the electrolyte [4] and also shields the area which is being investigated [5].

In submicrometre level studies of nucleation, changes in morphology and simultaneous electrochemical measurements provide fundamental insight into electrochemical phenomena [6–8]. The techniques have also found applicability in the study of processes of technological interest including metal deposition on printed circuit boards and electrodeposition by pulse plating [9, 10].

To gain a better understanding of the fundamentals of reversible processes, investigations have been carried out on copper electrolyte/noble metal systems: Cu/Cu [7], Cu/Au [6] and Cu/Pt [8]. The nucleation and growth compare well with 3D nucleation theory when the applied cathodic overpotential is large but *in situ* AFM results have shown that a more detailed theory is needed especially at lower cathodic overpotentials [8]. For copper on noble metal crystalline surfaces at sites of surface imperfections including steps and kinks [6, 8, 11, 12]. On polycrystalline gold surfaces, at small cathodic overpotentials, copper also grows from surface imperfections. At intermediate stages of copper crystals grow in parallel with the plane of the surface [13].

In the present work, copper was electrodeposited on gold at low cathodic overpotentials and followed by *in situ* STM as the growth proceeded. A 59 ± 5 mV separation was observed between onset of copper deposition and end of dissolution which indicates a single electron process. On the basis of *in situ* STM images and of current–voltage diagrams a mechanism of copper electrodeposition is discussed. Finally, the influence of the tip potential on the electrode processes is presented.

2. Experimental details

2.1. *Instrument*

The measurements were carried out at room temperature using a commercial scanning tunnelling

* Present address: Chemical Laboratory A, The Technical University of Denmark, Building no. 207, DK-2800 Lyngby, Denmark.

0021-891X © 1996 Chapman & Hall

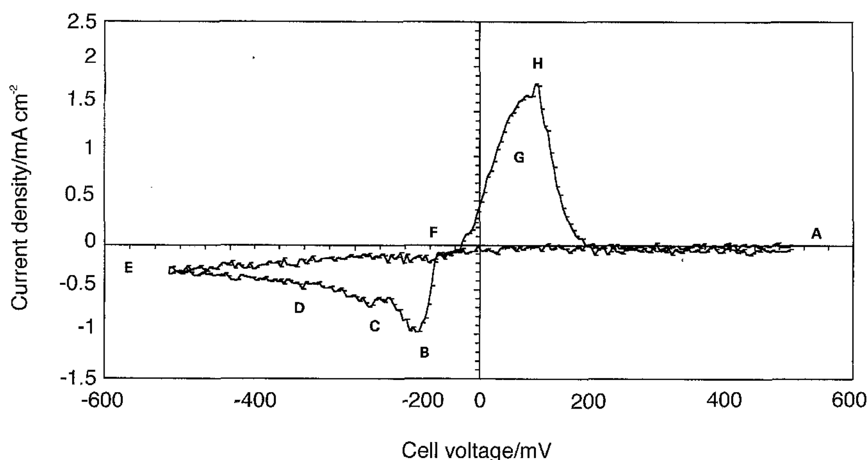

Fig. 1. Current–voltage diagram for the polycrystalline gold surface in acidified copper sulphate (0.01 M $CuSO_4$, 0.01 M H_2SO_4) at a sweep rate of $1\,mV\,s^{-1}$. The sweep of potential is carried out in the direction going from A to E via B, and back to A via F and H. See text for explanation of details A–H.

microscope (STM) (Danish Micro Engineering-Rasterscope^{TM} 3000) modified for electrochemical studies. Separate computers (PCs) were used for the STM controller and for the electrochemical cell. This arrangement is advantageous for the design of special electrochemical experiments such as those required in the study of pulse plating [10] because the cell and the computer software can then be easily altered independently. Both the tip potential (E_t) and the potential of the working electrode (E) can be controlled independently with respect to a common reference electrode by means of a bipotentiostat (EC-Rasterscope^{TM}). This allows imaging of electrochemical processes *in situ* from the atomic level to areas of $6\,\mu m \times 6\,\mu m$. Any influence of mechanical vibration on the scanning was damped by placing the electrochemical cell on a heavy platform hanging by rubber wires attached to the ceiling. The piezoelectric scanner and cell were placed under a glass bell jar. The air under the bell jar was kept saturated in water vapour with respect to the electrolyte to prevent evaporation and to prevent temperature fluctuations.

2.2. *Cell*

The electrochemical cell consisted of a vacuum evaporated gold film (working electrode area: $0.5\,cm^2$) on borosilicate glass $10\,mm \times 10\,mm$ (Berliner Glas AG) and a teflon coated Viton O-ring. A 1 mm Pt wire which was flame heat-treated prior to an experiment was applied as the counter electrode and the (pseudo)reference was a 0.2 mm copper wire (Cu/Cu^{2+}, $E_{Cu/Cu^{2+}} = E_{SHE} + 277\,mV$) which was etched in 4 M HNO_3 and cleaned in Millipore water. Before the reference electrode was used it was kept in contact with the electrolyte for a period of stabilization. The electrolyte was 0.01 M $CuSO_4$ (Riedel-De Häen, p.a.); 0.01 M H_2SO_4 (Merck, p.a.) in Millipore water; the volume was $150\,\mu l$.

The current–voltage diagrams were recorded at a sweep rate of $1\,mV\,s^{-1}$. The sweep rate was kept low for two reasons. (i) To maintain a high quality *in situ* STM image at all potentials. If the sweep rate was $> \sim 1\,mV\,s^{-1}$ the image was most commonly observed to have horizontal stripes which blurred the image features. (ii) The electrode kinetics are relatively slow and small current densities ensure that the electrode processes proceed almost uniformly over all the surface area of the working electrode.

2.3. *Tip*

It has been shown that the sides of the tip (Pt/Ir) must be carefully coated by an insulating material leaving only $10^{-6}\,cm^2$ or less exposed to the electrolyte for the conduction of tunnelling currents [14]. The insulation of the tip diminishes the faradaic current contribution to the total tip current and thus facilitates the imaging. By applying the electropaint method [14] (Electropaint: ZQ 8-43225, BASF) the tip faradaic current was suppressed to below 1 pA at fixed potentials, E, (or cell voltages, E_{cell}) in the range $-500\,mV < E < 500\,mV$. As reported previously [10] the quality of the images obtained by *in situ* STM (i.e., the signal-to-noise level) is largely dependent on the quality of the tip coating. The major part of the noise originates from the tip faradaic current which adds to the tunnelling current. For tunnelling currents in the range 1–250 nA and with a fixed electrode potential, the tip faradaic current should be less than 100 pA [14]. In this work tunnelling currents were in the range 1–10 nA. To maintain *in situ* STM images of high quality during a sweep of the electrode potential, it was found that the tip faradaic current should be kept below 0.1% of the tunnelling current. The low noise level then allowed imaging of any electrode process of interest as it proceeded (provided that no metal deposition took place on the tip).

The images were acquired in the constant current mode (1–10 nA) and all images were slightly filtered so as to sharpen all features. The images presented in Figs 2–5 were recorded starting from the lower part of the image proceeding towards the top.

3. Results

3.1. *Current–voltage diagram* (*Fig. 1*)

Significant features of the response in current to the change in potential are indicated by the letters A–H

in the Figure. From A towards B and down to about $-30\,mV$ no changes visible to the naked eye occurred on the gold surface. At B ($E = -100\,mV$) the major part of the copper was electrodeposited and the potential of the reference electrode changed accordingly. Also, at this stage of electrodeposition the surface adopted the bright red colour of copper. Continuing to C the copper surface appeared to tarnish, and the colour changed from bright red to pale red. When the potential was lowered further going from C towards D and E the colour of the surface gradually darkened. At potentials below about $-500\,mV$ the colour of the surface appeared dark red, hydrogen evolution occurred for $E < -400\,mV$. By increasing the potential again from $E = -500\,mV$ towards F the colour of the surface changed gradually from dark red to a colour reminiscent of pure copper. As the potential approached the region G all the copper was dissolved while at H gas bubbles were observed and the colour of pure gold was recovered. The characteristics of the current-voltage diagram of Fig. 1 were obtained while the *in situ* STM scanning was proceeding. Except for one minor feature, they did not differ from the characteristics of current–voltage diagrams obtained without the STM tip in the electrolyte involving a small noise spike at H. The appearance of the spike coincides with the potential of gas evolution, presumably hydrogen. Possibly, the current spike at H is due to the tip momentarily touching the surface as the gas evolves. The evolution of gas may account for the high current density which exceeds the limiting current density of the system. The overall shapes of the current–voltage curves for the present system resemble well cyclic voltammetry curves for similar electrochemical systems investigated by AFM [12, 15]. For current–voltage diagrams which were recorded after the first cycle of copper electrodeposition/dissolution major changes in features (current peak heights as well as potential positions) were observed (not shown). These changes have been related to a copper–gold alloy formation during the first cycles of copper electrodeposition/dissolution [17].

3.2. *Investigation of copper electrodeposition by in situ STM*

The initial stages of growth for the electrodeposition of copper were followed on a fresh polycrystalline gold surface (Fig. 2(a)–(d)). The image in Fig. 2(a) shows the characteristics of the fresh surface; this surface was maintained by fixing the potential at $E = +400\,mV$ where no current flows. When the potential is gradually lowered to $E = -20\,mV$ the onset of copper growth is observed as a formation of copper nuclei which after a few minutes in the region of rising cathodic current just before B cover the entire surface (Fig. 1 and Fig. 2(b)). The copper nuclei of Fig. 2(b) consist of hemispherical growths with a characteristic diameter of 30 nm. When fixing the potential at $E = -20mV$ the image features of Fig. 2(b) change no more after 10 min and no more copper deposits. Although the image area of the gold surface was fully covered by copper at $E = -20\,mV$, only a fraction of the available copper ions in the electrolyte had been deposited. This was demonstrated by lowering the potential further to $E = -30\,mV$ when more copper was electrodeposited (Fig. 1 and Fig. 2(c)). With the potential fixed at $E = -30\,mV$ more layers of copper nuclei form and flakes of crystalline copper start to appear. The characteristic area of the copper flakes varies between $0.01\,\mu m^2$ (Fig. 2(c)) and $0.1\,\mu m^2$ (Fig. 2(d)). The images of Fig. 2(c) and (d) were recorded consecutively revealing the change of surface morphology as a function of time. By imaging the same area of the surface during half an hour it was seen that the surface morphology did not stabilise. At $E = -30\,mV$ the copper was constantly electrodeposited and electrodissolved [13]. The copper nuclei merged into flat copper crystals which gradually disintegrated to form copper nuclei again. By decreasing the potential further to $E = -45\,mV$ more copper was electrodeposited initially in the form of about 30 nm diameter copper nuclei. Also at $E = -45\,mV$ a balance between copper electrodeposition and dissolution was established (Figs 1 and 3(a)–(d)). In Fig. 3(a)–(d) is shown a sequence of four images which were recorded consecutively. During these four stages of the balanced situation the copper recrystallises. At the start of *in situ* STM scanning of the surface the lower part of the image (Fig. 3(a)) shows a sudden transition from copper nuclei to crystalline copper. The copper angular crystallite like particles (Fig. 3) are maintained only briefly, and during the sequence of Fig. 3(b)–(d) the crystalline copper breaks up into minor parts (Fig. 3(c)–(d)) finally arriving at another nuclei situation (not shown). It was found that states of the type shown in Figs 2 and 3 could be established at different fixed potentials down to $E = -100\,mV$ where no further growth of copper was observed.

3.3. *Anodic dissolution of copper investigated by in situ STM*

To study the anodic dissolution of copper, the cell voltage was first swept in the cathodic direction to $E_{cell} = -500\,mV$, at which potential bulk crystals of micron dimensions were observed (Fig. 4(a)). The morphology displayed in this image did not change as the potentials (E) increased from -500 to $-50\,mV$. For potentials approaching $E = 0\,mV$ the copper began to dissolve (Fig. 4(b)). The image in Fig. 4(b) shows the initial stage in the disintegration of the copper crystal where bits of copper move away from the crystal and dissolve. To investigate whether the balance between copper deposition and dissolution observed in the deposition process also appeared in the dissolution process, the potential was kept at $0\,mV$ for some minutes. After a few minutes the image stabilizes and it shows the surface covered with copper at $E = 0\,mV$ (Fig. 4(c)). Subsequent to the electrodeposition the copper layers may

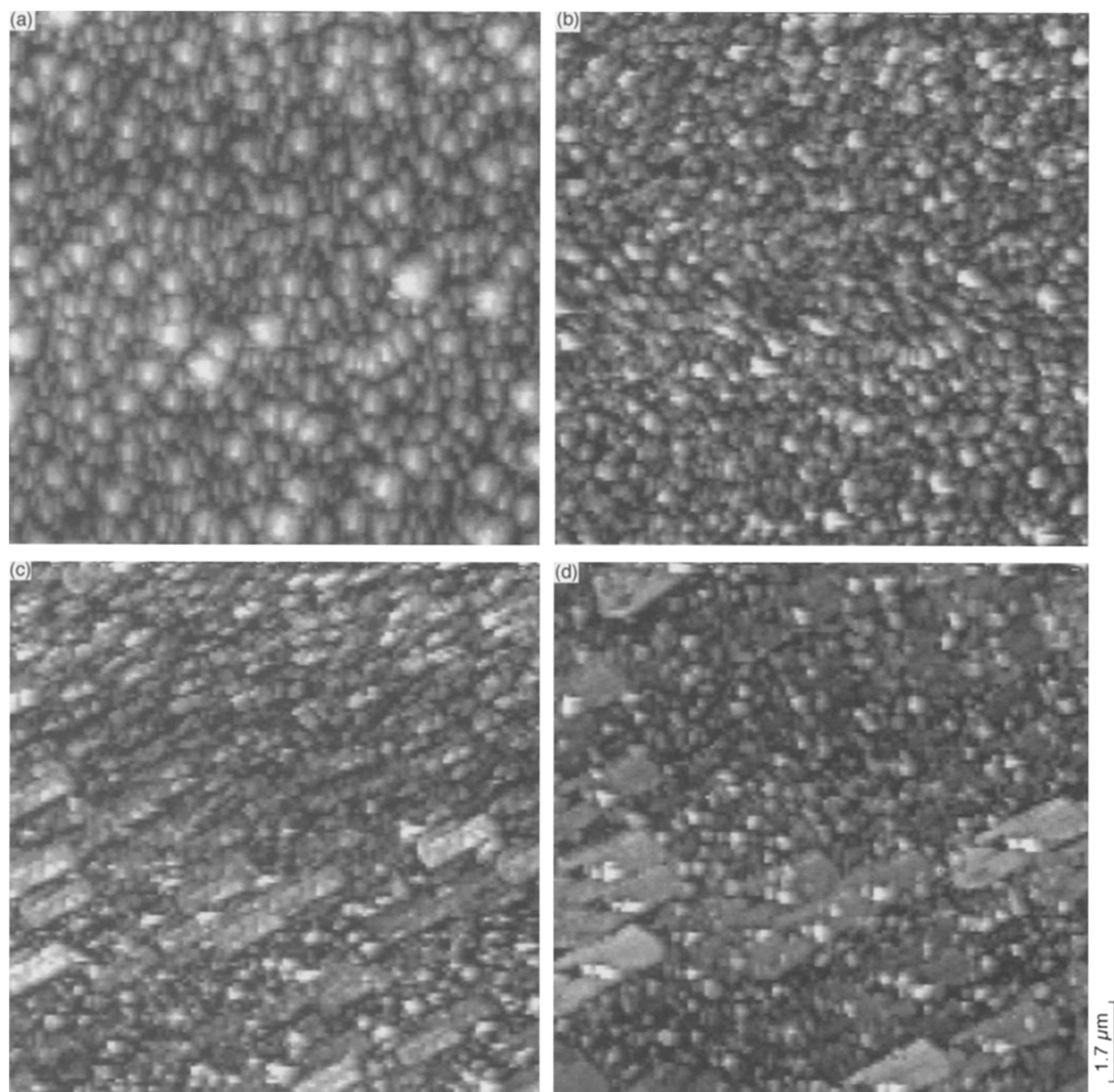

Fig. 2. Potentiostatic deposition of copper onto a clean pure gold surface in acidified copper sulphate (0.01 M $CuSO_4$, 0.01 M H_2SO_4) (a). Clean gold, $z = 45$ nm (z is the *in situ* STM depth scale); (b) Onset of copper electrodeposition, $E = -20$ mV, $E_t = +22$ mV, $z = 55$ nm (c)–(d). Balance between copper electrodeposition and dissolution at a fixed potential observed as a balance between copper nuclei formation and formation of copper crystals, $E = -30$ mV, $E_t = +12$ mV, $z = 50$ nm.

be removed successively from the surface by small increments in potential (E) from 0 to 25 mV (Fig. 1 (G) and Fig. 4(d)). A balance between copper precipitation and dissolution similar to that observed in the potential range $-60\,\text{mV} < E < -100\,\text{mV}$ during copper electrodeposition was not observed during these potential increments, i.e. in the potential range which corresponds to going from points F to G in Fig. 1.

3.4. *Influence of the tip potential*

To investigate the influence of the tip potential on surface morphology and on the potentials for copper deposition/dissolution a series of experiments were carried out at various tip potentials. Because this work was devoted to the study of bulk phenomena, electrodeposition by underpotential deposition (UPD) was not considered. Accordingly, for the present purpose, the onset of copper electrodeposition (E_{ON}) is defined as the potential where the gold surface (with area 850 nm × 850 nm) after a few minutes becomes covered with copper. Similarly, the end of anodic dissolution is defined as the potential (E_{OFF}) where all the copper is electrodissolved and the alloy gold surface is regenerated. These points are clearly identified by imaging and thereby following the surface morphology as a function of potential. For three different gold surfaces a total of 42 experiments was performed and the results are shown in Fig. 5(a) and (b). Clearly, both the onset of electrodeposition and the end of anodic dissolution are linearly dependent on the tip potential. It was found that neither the onset of electrodeposition nor the end of anodic dissolution were dependent on the

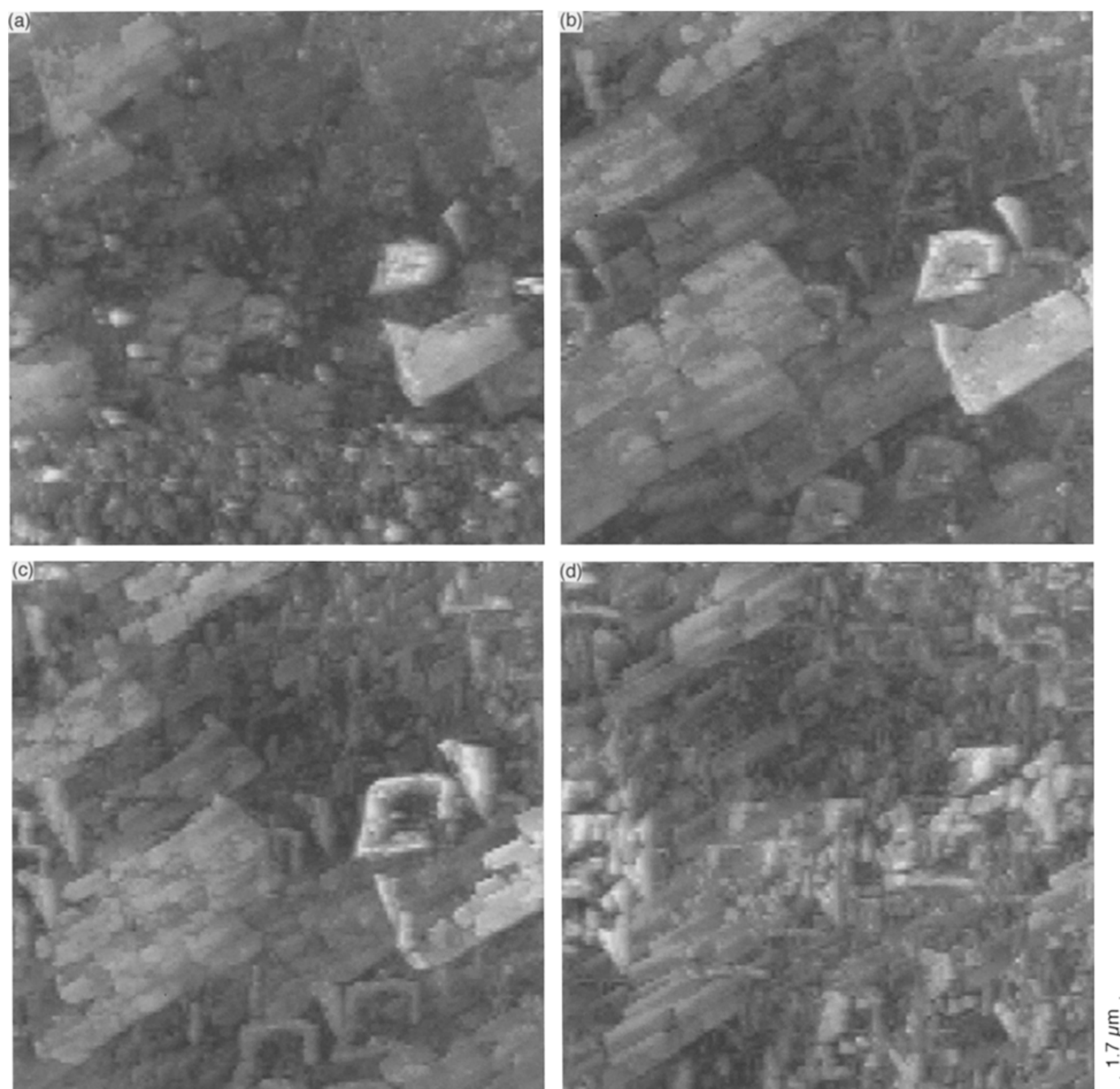

Fig. 3. Dynamics of copper electrodeposition and dissolution at a fixed potential shown by four images acquired consecutively, $E = -45$ mV, $E_t = -3$ mV. (a) An abrupt transition from nuclei to crystalline copper in the beginning of the image (lower part), $z = 50$ nm (z is the *in situ* STM depth scale); (b) an intermediate crystalline state of the copper morphology, $z = 40$ nm; (c) the copper crystalline flakes start to break into pieces, $z = 40$ nm; (d) the copper crystals just before they enter the nuclei state, $z = 35$ nm.

magnitude of the tunnelling current. However, when large tip potentials were applied it was necessary to increase the tunnelling current so as to retain the imaging during experiments such as those of Figs 5(a) and (b). Otherwise, the faradaic current would increase to a level where imaging was impossible. Furthermore, it was found that it was possible to retain the imaging at large tip potentials only when the tip potential was gradually increased from small values towards large values. The straight lines of Fig. 5 may be described by the linear relations:

$$E_{ON} = \alpha_{ON} \cdot E_t + E^0_{ON} \quad (1)$$

$$E_{OFF} = \alpha_{OFF} \cdot E_t + E^0_{OFF} \quad (2)$$

where α_{ON} and α_{OFF} are the slopes. E^0_{ON} and E^0_{OFF} denote onset and end potentials at zero tip potential, respectively. By fitting the data to a straight line the following values are found for $E_t > -87 \pm 3$ mV:

$$\alpha_{ON} = 0.505 \pm 0.003 \qquad E^0_{ON} = -57.3 \pm 1.8\,\text{mV}$$

$$\alpha_{OFF} = 0.502 \pm 0.007 \qquad E^0_{OFF} = 2 \pm 5\,\text{mV}$$

(i.e., E^0_{OFF} is not significantly different from zero).

For $E_t < -87 \pm 3$ mV the onset of electrodeposition was always observed at $E = -101 \pm 1$ mV (Fig. 5(a)). However, the end of dissolution was not well defined but occurred at approximately $E = -15$ mV (Fig. 5(b)), and no evidence of balance between copper electrodeposition and dissolution could be found in the images. All dissolved copper could be deposited at $E = -101$ mV for $E_t < -87$ mV. The determination of the onset of deposition and end of dissolution at negative tip potentials and negative potentials of the

Fig. 4. Anodic copper dissolution. (a) Large copper crystals grown by sweeping the potential (E) from +400 to −100 mV with a sweep rate of 1 mV s^{-1}, $z = 190$ nm (z is the *in situ* STM depth scale); (b) the copper dissolution starts at $E = 0$ mV, $z = 155$ nm; (c) 5 min after the copper dissolution started, $E = 0$ mV, $z = 40$ nm; (d) further copper dissolution at $E = +25$ mV, $z = 40$ nm.

working electrode were impeded by a simultaneous electrodeposition of copper on the tip and on the gold surface; this deposition greatly disturbed the imaging. The lines in Fig. 5(a) and (b) have the same slope and their spacing (i.e., the difference between onset of electrodeposition and end of anodic dissolution) is 59 ± 5 mV for $E_t > -87 \pm 3$ mV.

4. Discussion

4.1. *Electrodeposition and dissolution of copper*

When utilising current–voltage diagrams [16] in connection with *in situ* STM a balance has to be considered between the very local information obtained by *in situ* STM and the surface average information gained from current–voltage diagrams [7]. It has been suggested that for electrodeposition of bulk copper on polycrystalline gold surfaces an area of 10^4–10^5 nm^2 is suitable [13]. If the area is small (high resolution) it is very likely that the initial nucleation and growth would occur outside the frame of imaging. Thus, in this work relatively large surface areas are imaged (Figs 2–4). The balanced situations of Fig. 2(b)–(d) and 3(a)–(d) correspond to the potential range where the process is reversible and where the activity of the copper ions in solution is not significantly changed, that is, the potential of the reference electrode may be considered constant in this range. Assuming equilibrium between Cu^{2+}, Cu^{+} and Cu at the electrode surface,

$$Cu^{2+} + Cu \rightleftharpoons 2Cu^{+} \quad (3)$$

for $k = 10^{-6}$ [18], the following calculation can be made.

By counting the number of nuclei in the image of Fig. 2(b) the nuclei density was estimated to be 3×10^{10} cm^{-2} which, of course, is a slightly too low

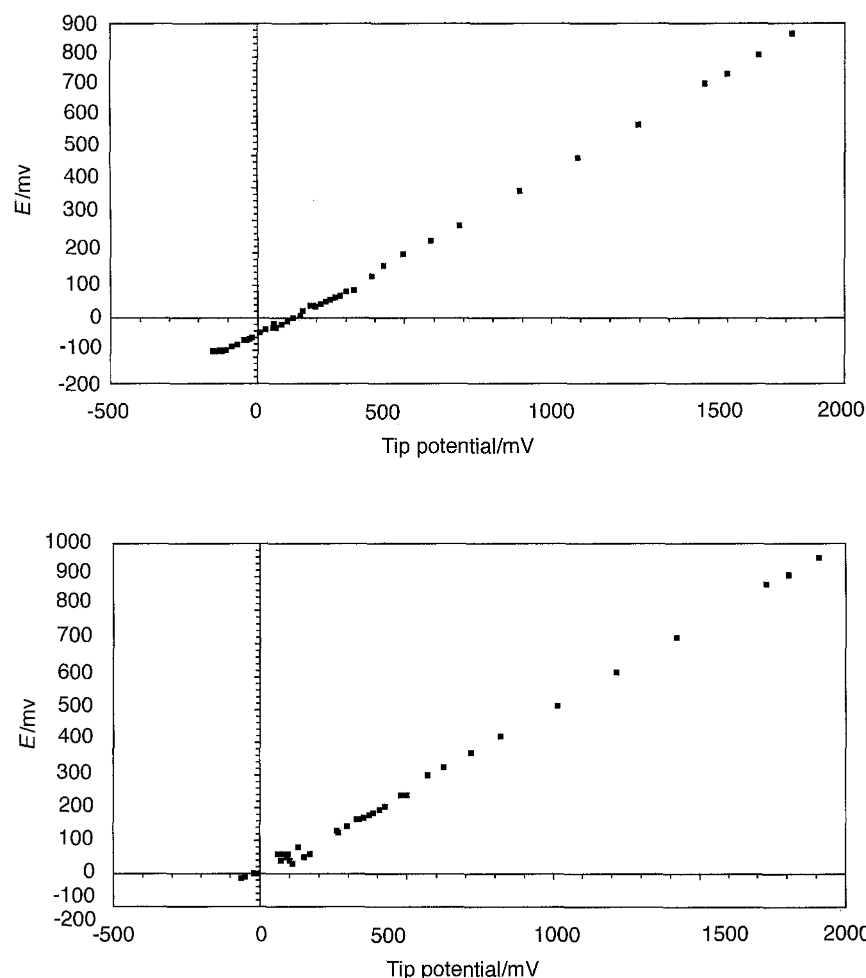

Fig. 5. Influence of the tip potential on the electrochemical process. (a) The points mark the onset of copper electrodeposition as imaged by *in situ* STM; (b) the points indicate the end of copper dissolution where the original area of the gold surface was recovered.

number because only visible nuclei are counted. However, the density compares with that found in other investigations [11]. The number of copper atoms in one spherical copper nuclei with an average diameter of 30 nm is 1.2×10^6 (assuming bulk copper density $8.93\,g\,cm^{-3}$). The number of cuprous ions in the electrolyte adjacent to the electrode (area: $0.5\,cm^2$), for an electrolyte with $[Cu^{2+}] = 0.01\,M$, is $6 \times 10^{16}\,cm^{-2}$ (neglecting double layer effects). This is 2×10^6 times larger than the number of copper nuclei, and considering the approximations involved, corresponds to the above estimate of the number of atoms in a nucleus (2×10^6 and 1.2×10^6). This suggests that the first copper nuclei are formed at low cathodic overpotentials and solely by reduction of cuprous ions. In addition, the validity of the above equilibrium requires that the copper phase on the gold electrode is in equilibrium with the ionic species; this explains the balance between copper deposition/dissolution observed at fixed potentials (Figs 2(a)–(d) and 3(a)–(d)).

The process of initial nucleation involves formation of 3D nuclei at surface imperfections; the dimensions of the nuclei increase by 3D growth until the surface is covered with copper (Fig. 2(b)) in agreement with earlier reports [6–8, 10, 11]. At slightly higher cathodic overpotentials the density of copper on the surface increases to form crystals (Figs 2(c)–(d) and 3(a)–(d)). The formation of crystals may be a result of either surface diffusion of copper atoms or a balance between copper deposition and dissolution. The balance between electrodeposited copper nuclei and crystalline copper flakes at fixed potentials (Figs 2(c)–(d) and 3(a)–(d)) shows that the surface density of copper exhibits large local variations. In the images of Fig. 2(c)–(d) the number of nuclei decreases when the crystals grow, suggesting that a constant amount of copper is present at the metal surface at a fixed potential.

In the presence of small amounts of organic additives, such as crystal violet or benzothiazole derivatives, initial nucleation is also observed at sites of surface imperfections [11], but there is lateral growth rather than 3D growth [5, 9, 11]. Although 3D growth dominates in the initial process of nucleation and growth, some degree of lateral growth may be induced by fixing the potentials (Figs 2(b)–(d) and 3(a)–(d)). The lateral growth and disintegration into nuclei as a function of time may be caused by local variations, the density of copper deposition possibly being induced by fluctuations of the potential of the reference electrode. Alternatively, the abrupt changes in copper morphology which extend to all the area of the image (Fig. 3(a)) may be related to the influence of the tip which stabilizes the potential distribution locally.

Dissolution of copper is characterized by an initial rapid change of copper morphology from large crystals of micrometre size (Fig. 4(a) and (b)) to one of faceted structures (Fig. 4(c) and (d)). The faceted structures also appear on pure copper surfaces which

are polarised anodically in electrolytes of perchloric acid [7] or in sulphuric acid [19] which indicates that the copper on gold is comparable to a polycrystalline copper surface during dissolution. The end of copper dissolution was observed at a potential 59 ± 5 mV above the onset of deposition (Fig. 5(b)), that is, at a potential which occurred significantly below the peak potential of the anodic peak (Fig. 1, H). When the electrode potential and the tip potential were fixed anywhere in the range between the two lines of Fig. 5(a) and (b), a constant amount of copper resided on the surface. These observations show that bulk copper is deposited and dissolved within the potential range between B and G in Fig. 1 and suggest that, especially, the anodic peak underneath H does not reflect a simple process of copper oxidation. This aspect will be explored in a future study.

4.2. *Tip effects*

Electrodeposition of copper has been studied by *in situ* STM at low tip potentials which facilitates the imaging [11], in the potential range around zero in Fig. 5(a) and (b). If the tip potential is changed during the scanning, clearly, from Fig. 5(a) and (b) the potential at which the electrode process occurs is affected. Thus, the imaging by *in situ* STM actually influences the electrochemical process. The increasing overpotential of electrodeposition and dissolution as a function of tip potential (Fig. 5(a) and (b)) is explained as the result of copper ions being electrostatically repelled by the tip at high potentials [5]. It was only possible to follow the processes at the gold electrode up to such high tip potentials (beyond the potential of oxygen evolution for the tip) by applying tips which exhibit faradaic currents less than 1 pA. Because the straight lines of Fig. 5(a) and (b) are parallel it is demonstrated that the influence of the tip on the electrode process can be considered simply as a change in reference potential. The results presented in Fig. 5(a) and (b), together with those of Fig. 1, show that the *in situ* STM technique probes the processes at the electrode very locally. As the current-voltage diagram in Fig. 1 was unaffected by change of tip potential, it must be considered how the imaging can be applied together with other electrochemical methods to extract information about mechanisms of electron transfer. Some information can be obtained by inspection of Fig. 5(a) and (b). The slope (α of Equations 1 and 2) is 0.504 ± 0.008 and is a direct measure of the tip local influence on the electrochemical process. At $E_t = 0$ it is found that $E = -57 \pm 2$ mV which corresponds to the onset of bulk copper electrodeposition (Fig. 5(a)) with the faradaic processes at the tip being at equilibrium (i.e., the tip faradaic current is zero). Accordingly, the true onset of copper electrodeposition with minimum influence of the tip, as defined in the results section, occurs at $E = -57 \pm 2$ mV. Thermodynamically, the onset of copper electrodeposition is expected to occur at $E = 0$ mV (without the influence of the tip) [16] but this was observed in the present work only when the tip potential was $E_t = 113$ mV (Fig. 5(a)). In other investigations of bulk copper electrodeposition the onset has not been reported to occur at $E = 0$ mV vs Cu/Cu^{2+} and, for copper deposition on Pt in a relatively concentrated electrolyte, the critical potential for copper nucleation was observed at an overpotential of 120 mV vs SSE [8]. The deviation from the thermodynamic prediction is related to the fact that bulk deposition is an activated process of nucleation and growth which requires a significant overpotential for nucleation [5, 11]. Obviously, there is a need to clarify at which potential bulk copper electrodeposition is initiated in different electrolytes. If the onset of copper electrodeposition must occur at $E = 0$ mV according to thermodynamics, then, for the present system the electrodeposition might be impeded by kinetic factors and copper would be observed only after a long time. Furthermore, the initial nucleation process at $E = 0$ mV might have occurred outside the frame of imaging. The end of dissolution was observed at $E = 0$ mV (and zero tip potential) (Fig. 5(b)) in accordance with thermodynamics.

For large cathodic tip potentials copper electrodeposition was always observed at $E = -101 \pm 1$ mV. The potential $E = -101$ mV corresponds in Fig. 1 to the point B, which is associated with the point where all the copper has been electrodeposited. Applying $E = -101$ mV to Equation 1 yields $E_t = -87 \pm 3$ mV (Fig. 5(a)), which is interpreted as the tip potential where copper is electrodeposited on the tip. Similarly, the copper anodic dissolution at the tip occurs at $E_t = -30 \pm 6$ mV (Fig. 5(b)). At $E_t = 0$ the potential for termination of copper dissolution is $E = 0$ (Fig. 5(b)) but the anodic current has not reached its maximum at this point. Because the system is reversible [16] it is anticipated that the peak B (Fig. 1) at $E = -101$ mV is associated with an anodic peak of similar area and shape. Due to the symmetry of the current peaks in a reversible process the anodic current peak of copper dissolution is then expected to occur at $E = 12 \pm 2$ mV. Only 25–35% of the area under the peak H arises from the charge passed in copper dissolution.

The geometry of the tip can affect the interpretation of an image. It has been shown theoretically how multiple-tip effects can explain features in images with atomic resolution [20, 21]. For image acquisition in the range of atomic resolution it is important that the tip is sharp with a tip radius of curvature of only about 1 nm [22, 23]. In addition, it is important that the tip exhibits good conducting properties, which may be a problem especially in air measurements with tips made of non-noble metals. Because the tips for *in situ* STM measurements are coated by an insulating material [14] the tip radius of curvature which is exposed to the electrolyte is between 0.1 μm [24] and 1 μm [4]. Thus, the area exposed to the electrolyte is much larger than the area which mediates the tunnelling current [6]. Obviously, when the scanning is carried out the tunnelling part of the tip is kept to

within 0.1–1 nm of the sample surface and the remaining exposed part of the tip may then trap some electrolyte between the tip and the surface, forming a thin-layer cell [5]. This is expected to influence the electrochemical process under the tip; this is mainly because the tip prevents rapid diffusion of copper ions to or from the 'bulk electrolyte' to the electrolyte which is being investigated under the tip [4, 5]. The diffusive hindrance of copper ions by the tip may explain the results of Fig. 5(a) and (b); at high tip potentials copper is not electrodeposited within the frame of imaging, although it was deposited on the surface outside the frame of imaging at $E \simeq -100$ mV (as indicated by the current–voltage diagram, Fig. 1). At a certain tip potential ($E_t < -87$ mV, Fig. 5(a) and (b)) the shielding effect changes sign and the influence acting on diffusing copper ions becomes attractive was observed. Therefore, for $E_t < -87$ mV both the surface and the tip attract copper ions and the electrodeposition proceeds at the (limited) maximum diffusion rate.

4.3. *Electrodeposition on the recrystallised gold surface*

From *ex situ* studies of copper growth on copper at low cathodic overpotentials, it is well known that copper exhibits spiral growth [25]. We see very few indications of centres of spirals in the images (Figs 3–5). In Fig. 4(a) the bulk crystal in the top of the image may show the first turn of a growing spiral, but no growth centres were identified upon copper dissolution (Fig. 4(c)–(d)). The flatness of the copper surface is a general feature of bulk copper growth. Even from the initial stages of formation of crystallites at sites of surface imperfections, the top part of the crystal is planar (Figs 3–5) [8, 11, 25]. This corresponds well with *in situ* AFM investigations of bulk copper electrodeposition on Pt(1 1 1) where copper islands also have flat surfaces [8]. Planar surfaces of faceted deposits may extend over areas of 200 nm × 200 nm [26].

By polarizing Cu-rich gold alloys anodically it has been shown that a critical potential exists above which a de-alloying form of the corrosion occurs [27, 28]. The critical potential occurs at progressively lower positive potentials as the copper content in the alloy increases [27, 28]. Thus, if copper and gold form an alloy, observation of a critical potential in the current-voltage diagram may be expected as the potential is increased from cathodic potentials. From Fig. 1 it can be seen that the area under the curve near H (copper dissolution) is large compared with the area under the curve near B (copper deposition) and possibly some of this charge difference arises from de-alloying of a copper–gold phase. If a surface alloy were formed, and the present system regarded as a copper deficient copper–gold alloy [17], the critical potential would then be expected to occur at a large anodic potential [27, 28]. As the potentials were swept between −500 and 500 mV it is not unlikely that a critical potential may have occurred outside this potential range. Thus, the de-alloying of the presumed surface alloy then proceeded in the low overpotential regime, where copper dissolution is inhibited by a blocking action of gold atoms owing to their high surface mobility [27, 28]. Accordingly, if a copper–gold alloy were formed in the range of cathodic potentials [17] the thickness of the alloy layer would increase after each cycle of copper deposition/dissolution because copper dissolution is inhibited during the period of anodic polarization. This would explain the lack of a critical potential at high anodic potentials (Fig. 1).

5. Conclusions

(i) Growth of crystalline copper is observed in the initial stages of potentiostatic bulk copper deposition. The crystalline copper flakes are formed from copper nuclei which merge due to local variations in copper density. At low, fixed cathodic overpotentials in the range $-57\,\text{mV} < E < -100\,\text{mV}$ a balance between copper electrodeposition and dissolution is established.
(ii) The onset of bulk copper electrodeposition occurs at $E = -57 \pm 2$ mV and the end of bulk copper dissolution occurs at $E = 0 \pm 5$ mV (at zero tip potential) these potentials corresponding with features in the current–voltage diagram.
(iii) The technique of *in situ* STM probes the electrode processes only locally. The electrochemical process of copper electrodeposition on gold is dependent on the tip potential. For tip potentials below $E_t - 87$ mV (Cu/Cu^{2+}) copper deposition is initiated at $E = -101$ mV (Cu/Cu^{2+}) and copper is dissolved at $E \simeq -15$ mV. At tip potentials more positive than $E_t = -87$ mV the onset of bulk copper deposition is observed at $E_{ON} = 0.505 \times E_t - 57$ mV and the end of dissolution at $E_{OFF} = 0.502 \times E_t$.
(iv) In a wide range of potentials the difference in potential between onset of bulk copper deposition and end of dissolution was constant: 59 ± 5 mV. This potential indicates that the electrode process is a single electron process.

Acknowledgements

This work was financially supported by the Danish Materials Research Programme and Danish Micro Engineering A/S. Thanks are due to Dr Brücken (BASF, Germany) who provided the electropaint. The continued technical support from Dr C. E. Foverskov is gratefully acknowledged.

References

[1] A. A. Gewirth and K. J. Hanson, *Interface*, Spring (1993) 37.
[2] J. Wiechers, T. Twomey, D. M. Kolb and R. J. Behm, *J. Electroanal. Chem.* **248** (1988) 451.
[3] O. M. Magnussen, J. Hotlos, R. J. Nichols and R. J. Behm, *Phys. Rev. Lett.* **64** (1990) 2929.
[4] R. J. Nichols, D. M. Kolb and R. J. Behm, *J. Electroanal. Chem.* **313** (1991) 109.
[5] U. Stimming, R. Vogel, D. M. Kolb and T. Will, *J. Power Sources* **43–44** (1993) 169.

[6] D. M. Kolb, R. J. Nichols and R. J. Behm, 'Electrified Interfaces in Physics, Chemistry and Biology, (edited by R. Guidelli), NATO ASI Series C, (Kluwer Academic, Dordrecht, Netherlands (1992), p. 275.

[7] X. G. Zhang and U. Stimming, *J. Electroanal. Chem.* **291** (1990) 273.

[8] R. M. Rynders and R. C. Alkire, *J. Electrochem. Soc.* **141** (1994) 1166.

[9] R. J. Nichols, D. Schröer and H. Meyer, *Scanning* **15** (1993) 266–73.

[10] J. E. T. Andersen and Per Møller, *Surf. Coat. Technol.* **67** (1994) 151.

[11] R. J. Nichols, W. Beckmann, H. Meyer, N. Batina and D. M. Kolb, *J. Electroanal. Chem.* **330** (1992) 381.

[12] J. Y. Josefowicz, L. Xie and G. C. Farrington, *J. Phys. Chem.* **97** (1993) 11995.

[13] J. E. T. Andersen, G. Bech-Nielsen and P. Møller, *Surf. Coat. Technol.* **70** (1994) 87.

[14] C. E. Bach, R. J. Nichols, W. Beckmann, H. Meyer, A. Schulte, J. O. Besenhard and P. D. Jannakoudakis, *J. Electrochem. Soc.* **140** (1993) 1281.

[15] K. Kowal, L. Xie, R. Huq and G. C. Farrington, *ibid.* **141** (1994) 116.

[16] A. J. Bard and L. R. Faulkner, 'Electrochemical Methods', Wiley & Sons, New York (1980).

[17] J. E. T. Andersen and P. Møller, *J. Electrochem. Soc.* **142** (1995) 2247.

[18] G. W. Tindall and S. Bruckenstein, *Analytical Chem.* **40** (1968) 1402.

[19] B. J. Cruickshank, A. A. Gewirth, R. M. Rynders and R. C. Alkire, *J. Electrochem. Soc.* **139** (1992) 2829.

[20] H. A. Mizes, Sang-il Park and W. A. Harrison, *Phys. Rev. B* **36** (1987) 4491.

[21] J. F. Womelsdorf, M. Sawamura and W. C. Ermler, *Surf. Sci. Lett.* **241** (1991) L11.

[22] J. Tersoff and D. R. Hamann, *Phys. Rev. B* **31** (1985) 805.

[23] V. T. Binh and J. Marien, *Surf. Sci. Lett.* **202** (1988) L539.

[24] A. J. Bard, G. Denault, C. Lee, D. Mandler and D. O. Wipf, *Acc. Chem. Res.* **23** (1990) 357.

[25] H. Fischer, *Electrochim. Acta* **2** (1960) 50.

[26] M. J. Armstrong and R. H. Muller, *J. Electrochem. Soc.* **138** (1991) 2303.

[27] J. D. Fritz and H. W. Pickering, *ibid.* **138** (1991) 3209.

[28] T. P. Moffat, F.-R. F. Fan and A. J. Bard, *ibid.* **138** (1991) 3224.